small methods
www.small-methods.com

Cas9-Cleavage Sequences in Size-Reduced Plasmids Enhance Nonviral Genome Targeting of CARs in Primary Human T Cells

Ruirui Jing, Peng Jiao, Jiangqing Chen, Xianhui Meng, Xiaoyan Wu, Yanting Duan, Kai Shang, Liling Qian, Yanjie Huang, Junwei Liu, Tao Huang, Jin Jin, Wei Chen, Xun Zeng, Weiwei Yin, Xiaofei Gao, Chun Zhou, Michel Sadelain,* and Jie Sun**

T cell genome editing holds great promise to advance a range of immunotherapies but is encumbered by the dependence on difficult-to-produce and expensive viral vectors. Here, small double-stranded plasmid DNA modified to mediate high-efficiency homologous recombination is designed. The resulting chimeric antigen receptor (CAR)-T cells display a similar phenotype, transcriptional profile, and in vivo potency to CAR-T cells generated using adeno-associated viral vector. This method should simplify and accelerate the use of precision engineering to produce edited T cells for research and clinical purposes.

1. Introduction

The US FDA has approved four CD19-specific chimeric antigen receptor (CAR)-T products to treat several hematological malignancies. These products use either retroviral (RV) or lentiviral (LV) vectors to deliver CAR genes into primary human T cells.[1] Both RV and LV vectors integrate in semi-random fashion, resulting in variegated transgene expression and the risk of insertional mutagenesis.[2,3] In

R. Jing, P. Jiao, J. Chen, Dr. X. Meng, X. Wu, Dr. Y. Duan, K. Shang, L. Qian, Prof. J. Sun
Department of Cell Biology and Bone Marrow Transplantation Center of the First Affiliated Hospital
Zhejiang University School of Medicine
Hangzhou 310058, China
E-mail: sunj4@zju.edu.cn

R. Jing, P. Jiao, J. Chen, Dr. X. Meng, X. Wu, Dr. Y. Duan, K. Shang, L. Qian, Prof. J. Sun
Institute of Hematology
Zhejiang University & Zhejiang Engineering Laboratory for Stem Cell and Immunotherapy
Hangzhou 310058, China

R. Jing, P. Jiao, J. Chen, Dr. X. Meng, X. Wu, Dr. Y. Duan, K. Shang, Prof. J. Sun
Zhejiang Laboratory for Systems & Precision Medicine
Zhejiang University Medical Center
Hangzhou 310058, China

Y. Huang, Prof. X. Gao
Key Laboratory of Structural Biology of Zhejiang Province
School of Life Sciences
Westlake University
Hangzhou 310058, China

J. Liu, Prof. W. Yin
Key Laboratory for Biomedical Engineering of the Ministry of Education
College of Biomedical Engineering and Instrument Science
Zhejiang University
Hangzhou 310058, China

T. Huang, Prof. J. Jin
MOE Laboratory of Biosystem Homeostasis and Protection and Life Sciences Institute
Zhejiang University
Hangzhou 310058, China

Prof. W. Chen
Department of Neurobiology
Institute of Neuroscience
and Department of Cardiology of the Second Affiliated Hospital
Zhejiang University School of Medicine
Hangzhou 310058, China

Prof. X. Zeng
State Key Laboratory for Diagnosis and Treatment of Infectious Diseases
Collaborative Innovation Center for Diagnosis and Treatment of Infectious Diseases
and First Affiliated Hospital
Zhejiang University School of Medicine
Hangzhou 310058, China

Prof. C. Zhou
School of Public Health
and Sir Run Run Shaw Hospital
Zhejiang University School of Medicine
Hangzhou 310058, China
E-mail: chunzhou@zju.edu.cn

Prof. M. Sadelain
Center for Cell Engineering and Immunology Program
Sloan Kettering Institute
New York, NY 10044, USA
E-mail: m-sadelain@ski.mskcc.org

The ORCID identification number(s) for the author(s) of this article can be found under https://doi.org/10.1002/smtd.202100071.

DOI: 10.1002/smtd.202100071

contrast, genome editing can precisely insert genes at defined genomic sites using homology-directed repair (HDR).[4–7] Using CRISPR/Cas9 to insert a CD19-specific CAR at the T-cell receptor α constant (*TRAC*) locus will at once delete expression of the endogenous T cell receptor (TCR) and afford effective CAR expression, resulting in reduced T cell exhaustion and improved tumor rejection in a mouse model of leukemia.[8] Expression and regulation of *TRAC*-encoded CAR reduces tonic signaling, delays differentiation, and decreases exhaustion of T cells, enhancing potency of eradicating xenograft tumor.[8] Targeting different CARs as well as TCRs to *TRAC* locus showed similar enhancement compared to their virus-transduced counterparts.[9–12] Genome edited T cells may also be safer as TCR ablation minimizes the risk of autoimmunity and alloreactivity.[12,13] Thus, precise genome editing provides a generalizable strategy to enhance the safety and efficacy of T cell therapy.[14] However, the shift from random virus-based integration to precise CRISPR/Cas9-assisted insertion of CARs requires setting up a completely different T cell engineering platform.

The targeted integration of therapeutic genes needs the concomitant activity of three reagents, the CRISPR/Cas9 protein, a gRNA, and a donor DNA template. Plasmids expressing gRNA and Cas9 are effective in cell lines but have limited efficiency in T cells,[15] so instead Cas9 mRNAs/proteins and synthesized gRNAs are delivered into T cells by electroporation.[8–10,13] After Cas9/gRNA makes site-specific cleavage, an HDR template is required for precise knock-in of the CAR gene. Using adeno-associated virus (AAV) to deliver HDR template can achieve high knock-in efficiency, generating ≈20–45% edited T cell.[8,11,16] However, lengthy and expensive AAV production is a barrier to produce T cells for both research and clinical use.[17] AAV gene therapy also has potential genotoxicity.[18] Electroporated linear dsDNA has been explored as HDR template, producing ≈7–20% edited T cells.[9,10,14] In detail, 4 μg linear dsDNA were needed for each 10^6 T cells and the concentration has to reach 2 μg μL^{-1} for electroporation,[9,10] which can be achieved by pooling multiple PCR reactions with additional concentration steps. Even though producing linear dsDNA is easier and cheaper than AAV production, it is not as easy as extracting plasmid DNA from bacteria. Moreover, procedures to scale up PCR reactions and subsequent purification with Good Manufacturing Practices (GMP) to produce linear dsDNA have not been widely adopted for clinical applications yet. Meanwhile, large-scale GMP-grade plasmid manufacturing is commercially available and more economical than linear dsDNA manufacturing.[19,20] Thus, plasmid DNA, overcoming its current limitations, would be an ideal HDR template for both research and clinical use, provided that it could achieve comparable efficiency as linear dsDNA can.

2. Results and Discussion

Introducing two Cas9-cleavage sequences (CCSs) into HDR template plasmids has been shown to release the template by Cas9 and enhance knock-in efficiency in cell lines.[21] We first tested this strategy in 293T cells, introducing an N-terminal green fluorescent protein (GFP) fusion in the housekeeping gene *RAB11A*. There was a 75% increase of knock-in efficiency using template plasmids with two CCSs compared to those without CCSs, confirming previous findings[21] (Figure S1a,b, Supporting Information). Next we applied this strategy in primary T cells by co-delivery of Cas9/gRNA ribonucleoprotein (RNP) complex and CCSs-including plasmids (**Figure 1**a). As our goal was to generate TRAC-CAR-T cells, we cloned the HDR template (≈3.7 kb) for inserting a CD19-CAR at *TRAC* locus into the pUC57 vector (≈2.7 kb) with two CCSs (Figure 1a). Plasmids with two CCSs enhanced knock-in efficiency by 4.8-fold on average over plasmids without CCSs (n = 2, Figure S2a,b, Supporting Information). Since plasmid size affects the delivery efficiency by electroporation,[22] we deleted the *lacZ* module in the pUC57 backbone and generated a size-reduced vector (pMini, ≈1.6 kb) to carry the HDR template for CAR knock-in (Figure 1a). With this simple engineering, we can increase the knock-in efficiency by 8.6-fold on average, compared to pMini without CCSs (n = 4, Figure 1b,c). When T cells from different donors were sampled, CAR knock-in efficiency using pMini with two CCSs ranged from ≈10% to 16.8% (n = 11, Figure 1d). In detail, when CD4 and CD8 T cells were analyzed separately, the two populations showed similar knock-in efficiency (Figure S3a,b, Supporting Information). As plasmids with CCSs were also used for nonhomologous end jointing (NHEJ)-mediated knock-in,[23] we sequenced the *TRAC* locus of edited cells and found all knock-in events were HDR-mediated (Figure 1e,f). To compare the efficiency of our system with linear dsDNA-based nonviral method, we did a side-by-side knock-in test using linear dsDNA or plasmids with CCSs as HDR template while all other experimental parameters were kept the same.[9,10] Our results showed adding two CCSs to linear dsDNA significantly increased the efficiency (Figure S4a,b, Supporting Information). We next assayed the CCSs-containing template plasmids for GFP fusion at *RAB11A* locus. The on-target knock-in efficiency can reach 8–9%, while off-target integration was minimal (Figure S5a–c, Supporting Information).

Furthermore, our TRAC-CAR-T cells generated with template plasmids could be enriched from ≈10% to more than 50% 1 week after stimulation with antigen presenting cells (APCs) (**Figure 2**a). Such protocols to enrich CAR-T cells with APCs have been established for clinical use.[24] When different RNP and plasmid amounts were tested, no further enhancement was observed (Figure 2b,c). Next, we combined different strategies with the pMini vector to see if additional increase of knock-in efficiency could be achieved. As Cas9 with nucleus localization signals (NLSs) can help bring the template with CCSs into the nucleus, the number of CCSs in plasmids may affect the knock-in efficiency. When we systematically varied the number of CCSs in pMini from 0 to 3 (Figure 2d), we observed the highest efficiency with 2 CCSs (Figure 2e). Previous reports have suggested that homologous arm (HA) length can affect knock-in efficiency.[21] Therefore, we constructed HDR templates with HA length varying from 100 to 800 bp. Our results showed that they all had similar knock-in efficiency (Figure 2f). Moreover, *CCND1* gene was shown to further enhance the knock-in efficiency in cell lines.[21] When purified Cyclin D protein was electroporated together with Cas9/gRNA RNP and template plasmids, the knock-in efficiency was further enhanced by ≈18%

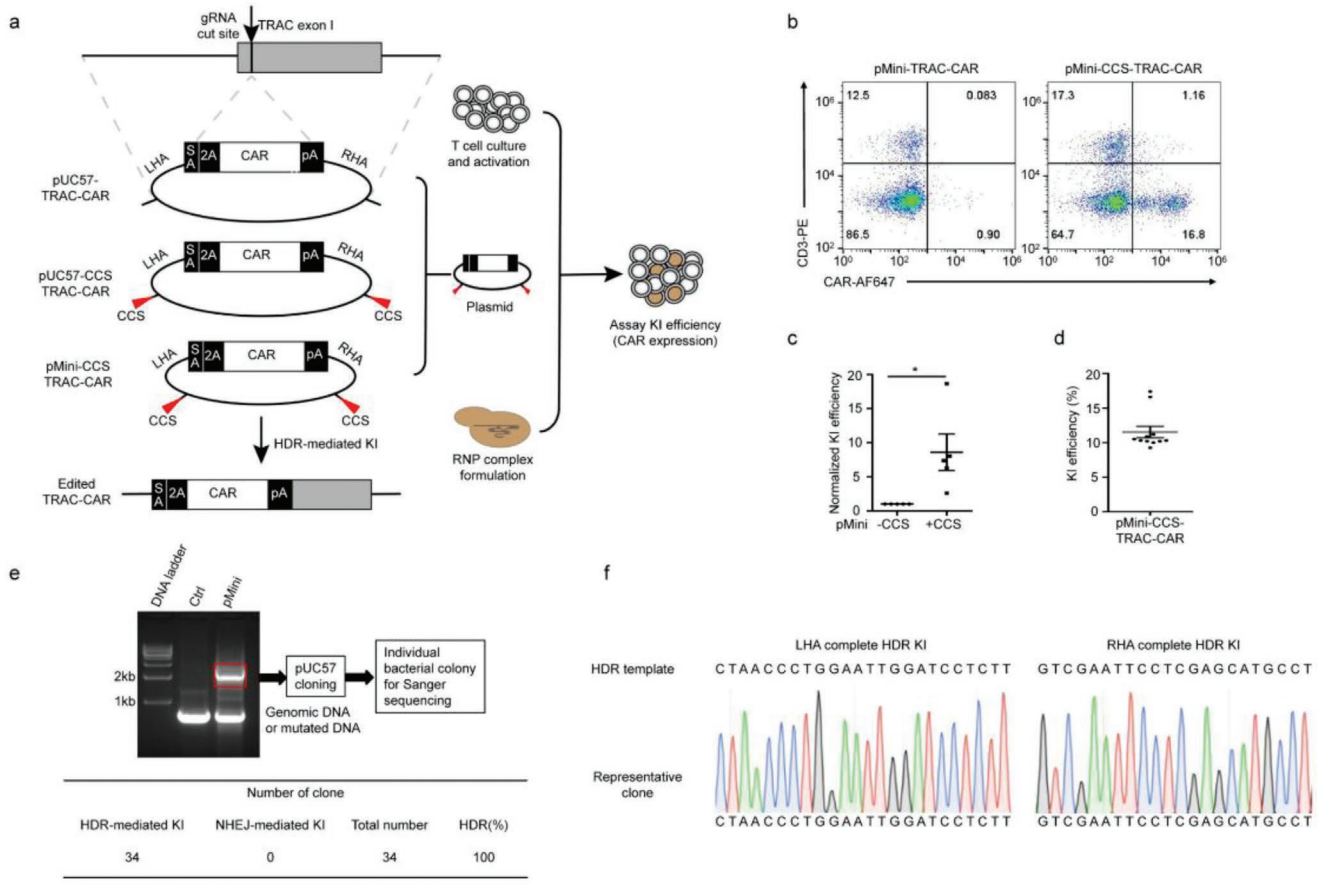

Figure 1. CRISPR/Cas9-mediated CAR knock-in (KI) with template plasmids in primary human T cell. a) Schematic of targeting a CAR to the *TRAC* locus with Cas9/gRNA RNP and different template plasmids. CCS, Cas9-cleavage sequence. SA: splice acceptor, pA: polyA tail, LHA: left homology arm, RHA: right homology arm. b) Representative flow plots of CAR KI with indicated plasmids as template. c) Averaged fold increase of KI efficiency with pMini-CCS-TRAC-CAR compared to pMini-TRAC-CAR plasmids ($n = 5$ donors). d) KI efficiency with pMini-CCS-TRAC-CAR averaged 11.7% ($n = 11$ donors). e) The PCR product of 2–3 kb size were cut off and cloned into pUC57 vector and individual bacterial colonies were picked for Sanger sequencing and summary of Sanger sequencing results. f) Alignment of sequencing result of a representative clone with expected HDR sequences at TRAC locus. Error bars represent SEM. $*p < 0.05$; $**p < 0.01$; $***p < 0.001$; ns, not significant (Student's *t*-test).

(Figure 2g). We used 2′-O-methyl 3′phosphorothioate (MS)-modified gRNA for all the experiments above as it was reported to be more stable than unmodified gRNA.[25] But it is more expensive, which could increase the manufacturing cost in clinical applications. Through side-by-side comparison, we found that MS-modified gRNA resulted in a 15% higher knock-in efficiency than unmodified gRNA (Figure 2h). Thus, we suggest using modified gRNA for T cell editing in research. But when editing large numbers of T cells in clinical settings, unmodified gRNA may be a cost-effective choice.

Next we assessed in vitro functions of these edited cells generated with plasmids (p-TRAC-CAR-T) and compared them vigorously with cells generated with AAV (AAV-TRAC-CAR-T). First, these p-TRAC-CAR-T cells kill $CD19^+$ target cells as well as AAV-TRAC-CAR-T cells (**Figure 3**a), which was reproducible in three donors. Second, both cells started to proliferate 3 days after electroporation with more than 85% viability (Figure S6, Supporting Information), and continue to expand in vitro in the absence of antigen, providing sufficient cells for xenograft tumor eradication and clinical use (Figure 3b). Third, we compared the long-term antigen-dependent proliferation in a weekly expansion assay with $CD19^+$ APCs. The number of p-TRAC-CAR-T cells lagged behind that of AAV-TRAC-CAR-T cells in the first 4 weeks, but started to catch up and after 6 weeks ended up higher (Figure 3c). The total 6 weeks expansion can generate as many as 1000 fold of cells. Fourth, we compared the genome-wide transcriptional profiles of p-TRAC-CAR-T and AAV-TRAC-CAR-T cells from two donors before and after antigen stimulation. Principal component analysis (PCA) demonstrated distinct clustering of CAR-T cells dependent on donor or stimulation status. However, p-TRAC-CAR-T and AAV-TRAC-CAR-T cells from the same donor before or after stimulation located closely, suggesting transcriptional similarity of these CAR-T cells (Figure 3d). In addition, p-TRAC-CAR-T and AAV-TRAC-CAR-T cells showed similar expression profiles of genes differentially expressed between effector and naïve/memory T cells[26] (Figure 3e and Figure S7, Supporting Information). Fifth, we used CyTOF mass cytometry to compare the phenotype (40 markers, Table S1, Supporting Information) of two types of CAR-T cells. *t*-Distributed Stochastic Neighbor Embedding (*t*-SNE) plot showed that p-TRAC-CAR-T and AAV-TRAC-CAR-T cells have comparable clustering patterns before

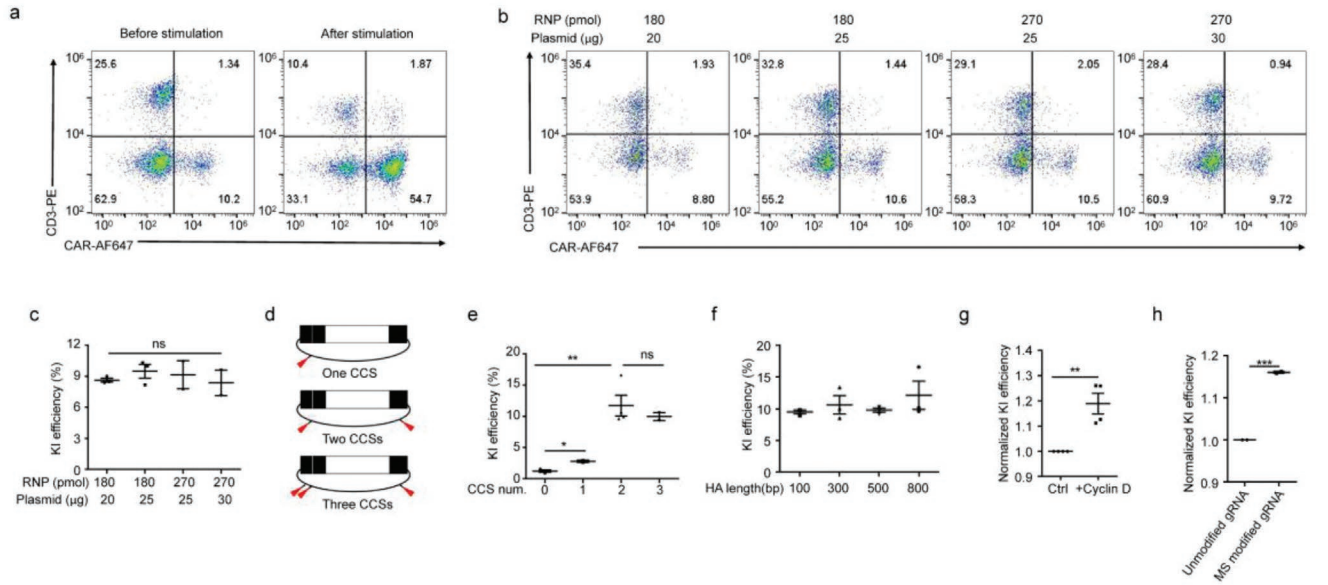

Figure 2. Optimization of CRISPR-Cas9-mediated CAR knock-in (KI) with template plasmids. a) Representative flow plots of CAR KI before or 1 week after stimulation with irradiated NIH/3T3-CD19 ($n = 3$ donors). b) Representative flow plots of CAR KI with indicated amount of RNP and pMini-CCS-TRAC-CAR plasmid. c) Averaged KI efficiency with indicated amount of RNP and template plasmid ($n = 2$ or 3 donors). d) Schematic of different CCS number located in pMini template plasmids. e) Averaged KI efficiency using pMini plasmids with indicated CCSs numbers ($n = 3$ donors). f) Averaged KI efficiency with indicated HA length ($n = 3$ donors). g) Averaged increase of KI efficiency with Cyclin D protein ($n = 4$ donors). h) Comparison of KI efficiency with normal guide RNA and MS guide RNA ($n = 2$ donors). Error bars represent SEM. $*p < 0.05$; $**p < 0.01$; $***p < 0.001$; ns, not significant (Student's *t*-test).

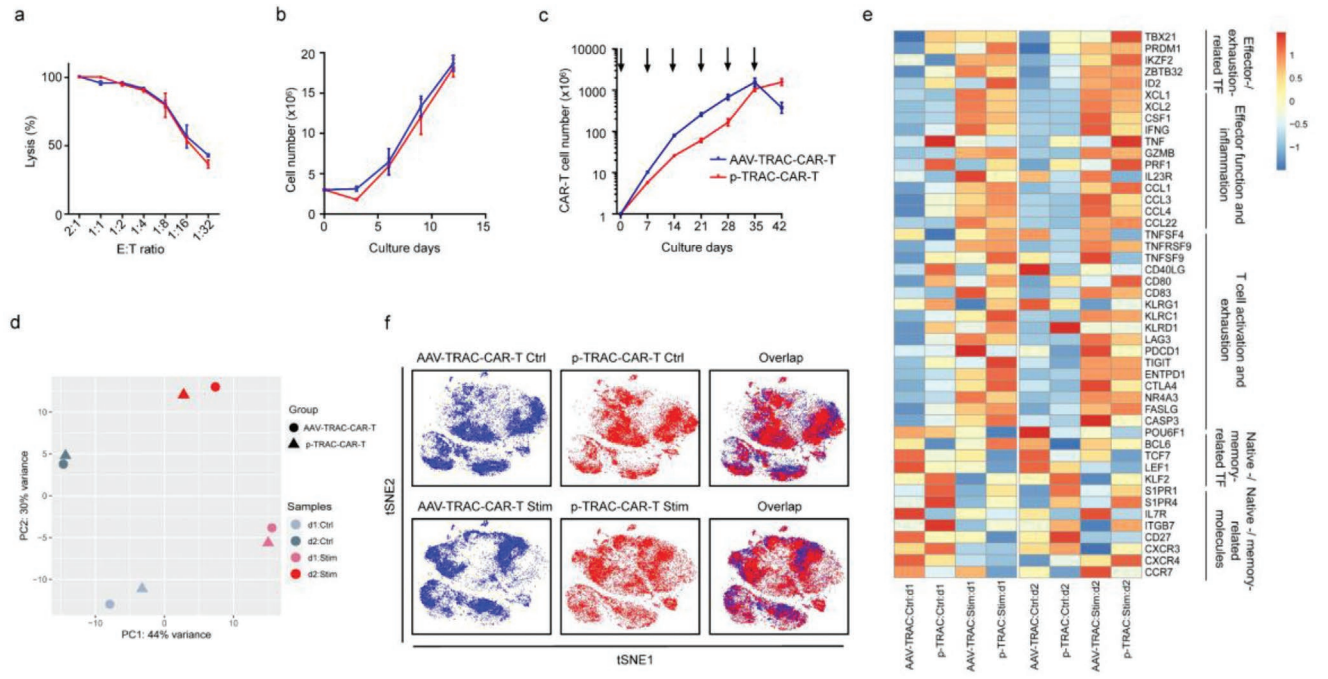

Figure 3. Functional comparison of edited TRAC-CAR T cells produced with plasmids or AAV as templates in vitro. a) Representative cytotoxic activity of CAR-T cells using an 18 h bioluminescence assay with FFluc-GFP Nalm6 as targets cells ($n = 3$ donors performed in triplicates). b) Representative cell counts of total T cells on indicated days after electroporation ($n = 2$ donors performed in triplicates). c) Representative cumulative cell counts of CAR-T cells upon weekly stimulation with irradiated NIH/3T3-CD19 cells ($n = 3$ donors performed in replicates). d) Principal component analysis (PCA) of global transcriptional profiles ($n = 2$ donors). e) Heat map demonstrating the expression profiles of indicated genes for different CAR-T cells ($n = 2$ donors); TF, transcription factor. (d1, donor 1; d2, donor 2, Ctrl, before antigen stimulation; Stim, 24 h after antigen stimulation.) f) t-SNE analysis of p-TRAC-CAR-T and AAV-TRAC-CAR-T cells measured by 40 markers with or without stimulation by NIH/3T3-CD19 cells.

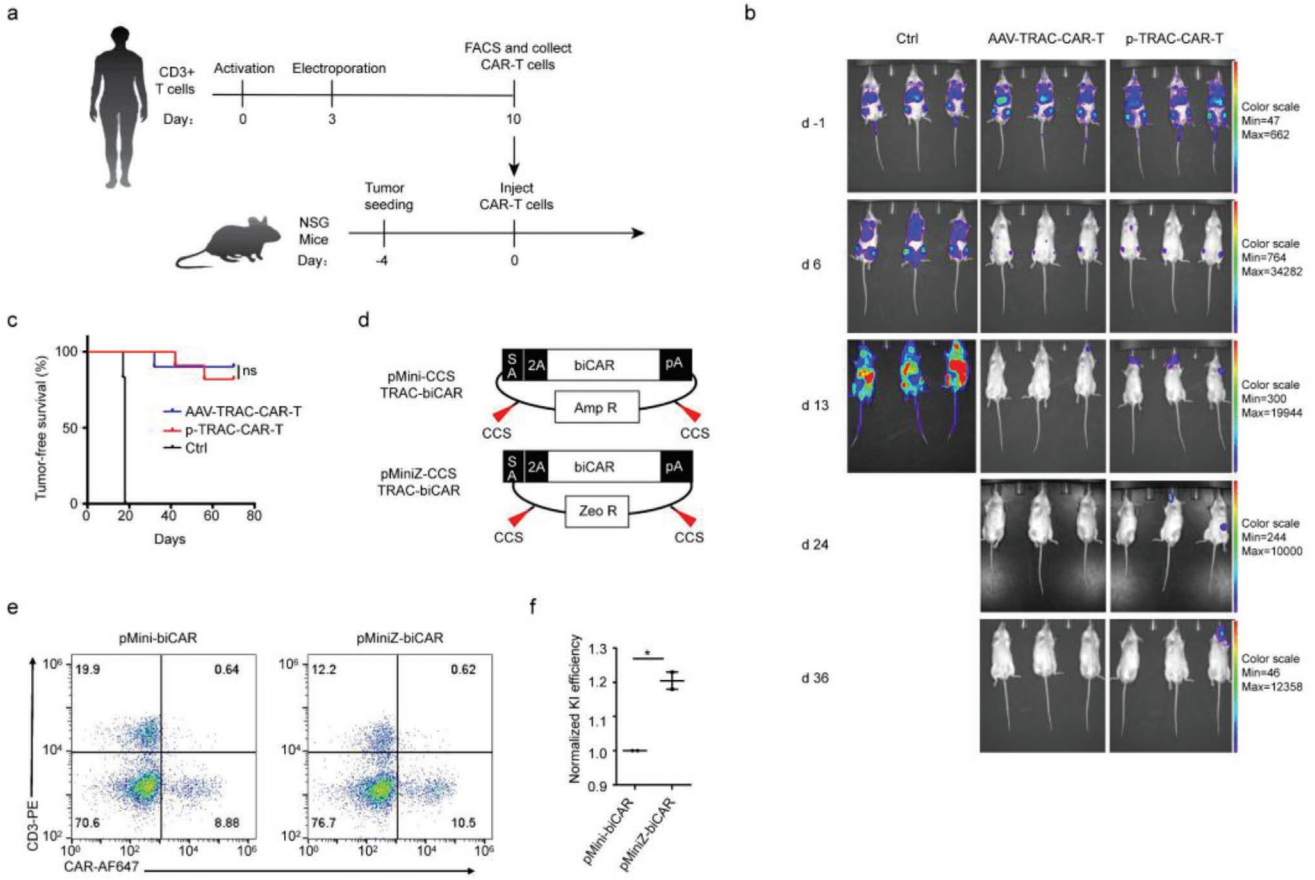

Figure 4. Functional comparison of edited TRAC-CAR T cells produced with plasmids or AAV as templates in vivo. a) Acute lymphoblastic leukemia tumor mouse xenograft model. NSG mice, nonobese diabetic (NOD)/severe combined immunodeficiency (SCID)/Il2rg−/− mice. b) Bioluminescent images of FFluc-GFP Nalm6-bearing mice treated with different CAR-T cells at indicated days (CAR-T cells were injected at day 0). c) Kaplan–Meier analysis of survival of mice treated with different CAR-T cells or untreated (Ctrl). (Ctrl: $n = 6$, AAV-TRAC-CAR: $n = 10$, p-TRAC-CAR: $n = 11$). d) Schematic of bispecific CAR in pMiniZ or pMini template plasmids with CCSs. e) Representative flow plots of bispecific CAR KI with pMini-CCS-TRAC-biCAR and pMiniZ-CCS-TRAC-biCAR. f) Averaged KI efficiency using pMini-CCS-TRAC-biCAR and pMiniZ-CCS-TRAC-biCAR ($n = 2$ donors). Error bars represent SEM. $^*p < 0.05$; $^{**}p < 0.01$; $^{***}p < 0.001$; ns, not significant (Student's t-test).

or after antigen stimulation, suggesting the phenotypical similarity of these two types of cells (Figure 3f). In detail, these differently made CAR-T cells showed similar levels of activation, differentiation, and exhaustion markers (Figure S8, Supporting Information).

Last, we tested in vivo antitumor function of CAR-T cells in an acute lymphoblastic leukemia mouse model (**Figure 4**a), where we injected the same low dose of AAV-TRAC-CAR-T cells and p-TRAC-CAR-T cells (1×10^5). In these "stress test" conditions, mice treated with different CAR-T cells showed no significant difference on the tumor burden (Figure 4b and Figure S9, Supporting Information) and long-term survival (Figure 4c), suggesting that both CAR-T cells had equally potent antitumor activity. On day 16 after CAR-T cell injection, equivalent number of CAR-T cells accumulated in the bone marrow. On day 36, there were more p-TRAC-CAR-T cells than AAV-TRAC-CAR-T cells accumulated, suggesting that p-TRAC-CAR-T cells may have a trend of longer persistence in vivo (Figure S10, Supporting Information, $n = 2$). The CAR we used above was a CD19-specific 1XX CAR developed for a range of clinical applications.[26] Since bispecific CARs have been shown to reduce relapse rate in clinical trials,[27,28] we tested whether a CD19 and CD22 bispecific CAR can be inserted at *TRAC* locus using the engineered plasmid pMiniZ (Figure 4d), which was generated by replacing the ampicillin resistance gene in pMini with the zeocin resistance gene to further reduce the vector size. Even though the bispecific CAR (≈2.2 kb) was about 50% larger than 1XX (≈1.45 kb), the knock-in efficiency still reached 10.5% with the pMiniZ template (Figure 4e), about 20% higher than that with pMini vector (Figure 4f).

3. Conclusion

We have thus developed a plasmid-based nonviral method to rapidly and inexpensively knock-in genes in primary T cells. We reduced the size of the plasmid and flanked the HDR template with two CCSs to achieve efficient knock-in. Plasmid edited CAR-T cells were as potent as cells produced with AAV template, which was shown to have superior tumor eradication compared to virus-transduced CAR-T cells. This new method simplifies the gene targeting in human T cells and makes use

of plasmid DNA that can easily be produced for clinical use. This approach will promote the use of precisely edited CAR-T cells for both research and clinical applications.

4. Experimental Section

Ethical Statement: In this study human peripheral blood mononuclear cells (PBMCs) were received from healthy volunteers with written informed consent and the protocol was approved by the Ethics Committee of Zhejiang University School of Medicine (Hangzhou, China, NO.2020-067). All animal experiments were approved by Institutional Animal Care and Use Committee of Westlake University (Hangzhou, China, AP#19-021-GXF).

Cell Lines and Culture Conditions: Nalm6 cells were transduced to express firefly luciferase (FFLuc)-GFP, cultured in complete RPMI (Gibco) medium with 10% fetal bovine serum (FBS, Vistech) and 1% penicillin/streptomycin (Gibco). NIH/3T3 cells were transduced to express human CD19 and cultured in Dulbecco's modified Eagle medium (DMEM, Gibco) medium with 10% FBS and 1% penicillin/streptomycin. 293T cells were cultured in DMEM medium with 10% FBS and 1% penicillin/streptomycin.

Isolation and Expansion of Human T Cells: Peripheral blood mononuclear cells were isolated by density gradient centrifugation from healthy volunteers' peripheral blood. Then T cells were purified using the Pan T Cell Isolation Kit (Miltenyi Biotec) and stimulated with CD3/CD28 T cell Activator Dynabeads (Thermo Fisher Scientific) with 1:1 cell to bead ratio and cultured in X-VIVO 15 serum-free hematopoietic cell medium (Lonza), supplemented with 10% FBS, 1% penicillin/streptomycin, 5 ng mL^{-1} interleukin-7 (IL-7), and 5 ng mL^{-1} interleukin-15 (IL-15) (Novoprotein). The cells were incubated at 37 °C, 8% CO_2. The medium was changed every 2–3 days, and cells were plated at 1×10^6 mL^{-1}. Human T cells were stimulated for 48 h, then debeaded for gene targeting experiments.

Plasmid Construction: gRNA expression vectors were constructed by cloning 20 bp oligo nucleotide target sequences into pX330 (Addgene plasmid #42230) containing a human codon-optimized SpCas9 expression cassette and a human U6 promoter driving the expression of the gRNA.

The pMini and pMiniZ vectors were modified from a pUC57 vector. LacZ and multiple cloning sites were deleted from pUC57 to construct the pMini vector. Then the ampicillin resistance gene sequence was replaced with zeocin resistance gene sequence to make the pMiniZ vector.

To generate template plasmids harboring Cas9-cleavage sequences (CCSs) flanking the homology arms, the gRNA target sequence together with a PAM sequence (NGG) was included in both the forward and the reverse primers for cloning templates into the pUC57, pMini, and pMiniZ vectors.

Protein Purification: Cas9 from *S. pyogenes* with two NLSs was subcloned from pX330 into a modified pET28b vector (Novagen), which contained an *N*-terminus 6 × Histidine SUMO tag. Recombinant fusion protein was expressed in the *E. coli* strain Rosetta (Novagen). After purification with a HisTrap FF column (GE Healthcare), the his-sumo tag was cleaved by ULP1 and subsequently removed by a second step HisTrap FF column purification. Cas9 protein was further purified by a heparin column and a Superdex 200 increase column on AKTA Pure (GE Healthcare). The protein was concentrated to 10 mg mL^{-1} and stored in a buffer containing 20×10^{-3} M 4-(2-hydroxyethyl)-1-piperazineethanesulfonic acid (HEPES) pH 7.5, 200×10^{-3} M NaCl, and 0.3×10^{-3} M *tris*(2-carboxyethyl)phosphine (TCEP) at −80 °C.

Human cDNA of CCND1 was cloned into a modified pET28b vector, which contains an *N*-terminus 6 × Histidine SUMO tag. Recombinant fusion protein was expressed in the *E. coli* strain Rosetta (Novagen). After purification with a HisTrap FF column (GE Healthcare), the his-sumo tag was cleaved by ULP1 and subsequently removed by a second-step HisTrap FF column purification. Cyclin D protein was further purified with an ion-exchange column (Source Q) and Superdex 200 increase column on AKTA Pure (GE Healthcare). The protein was concentrated to 10 mg mL^{-1} and stored in a buffer containing 20×10^{-3} M Tris–HCl pH 8.0, 200×10^{-3} M NaCl, and 0.3×10^{-3} M TCEP at −80 °C.

RNP Production: The crRNAs used in this paper were C*A*G*GGUUCUGGAUAUCUGU for *TRAC* locus, G*G*T*AGTCGTACTCGTCGTC for *RAB11A* locus. The same tracrRNA AGCAUAGCAAGUUAAAAUAAGGCUAGUCCGUUAUCAACUUGAAA AAGUGGCACCGAGUCGGUGCU*U*U*U was used (* 2′-O-methyl 3′phosphorothioate, MS). RNPs were produced by complexing two components: gRNA and Cas9 protein. In brief, crRNAs and tracrRNAs were chemically synthesized with MS modifications and annealed (Genescript). The annealing was set up in a reaction containing 30 µL RNase free H_2O, 20 µL annealing buffer (5X, 50×10^{-3} M Tris pH 8.0, 100×10^{-3} M NaCl), 25 µL crRNA (200×10^{-6} M), 25 µL tracrRNA (200×10^{-6} M), then heated at 95 °C for 5 min, gradually cooled to room temperature, aliquoted and lyophilized (Genescript). Lyophilized RNA was resuspended in RNase free water before use. 100×10^{-6} M gRNA in 10×10^{-3} M Tris pH 8.0, 20×10^{-3} M NaCl were then mixed by 1:1.25 volume with 40×10^{-6} M recombinant Cas9 (2:1 gRNA to Cas9 molar ratio) at room temperature °C for 20 min to form 22×10^{-6} M RNP complex. RNPs were then electroporated with template plasmids into T cells immediately after complexing.

CAR-T Cell Production: RNPs and template plasmids were electroporated into T cells 2 days after CD3/CD28 bead stimulation. Immediately before electroporation, debeaded T cells were centrifuged for 10 min, 1500 rpm, and resuspended in BTXpress Electroporation Solution (BTX). For each reaction, 3×10^6 cells were mixed with 8.1 µL (22×10^{-6} M, 180 pmol) RNPs and 7 µL (25 µg) template plasmids in a total volume of 100 µL and transferred to a 2 mm cuvette and electroporated with an AgilePluse system (BTX). Following electroporation cells were immediately transferred into culture medium. 2 h later, 5 ng mL^{-1} IL-7 and 5 ng mL^{-1} IL-15 were added. Then medium was changed every 2–3 days. For AAV-TRAC-CAR-T cells, 3.6 µL RNPs were incubated with 3×10^6 cells for electroporation. 30 min later, AAV virus (MOI = 1×10^5) (Vigene Biosciences, China) were added. 30 µg mL^{-1} cyclin D protein was co-electroporated with RNPs and template plasmids into human T cells. 7 days after electroporation, cells were harvested for fluorescence-activated cell sorting (FACS) analysis to determine the knock-in efficiency in each condition.

Determination of HDR-Mediated Knock-In by PCR and Sanger Sequencing: Human T cells were harvested 9 days after gene targeting for DNA extraction by FastPure cell/Tissue DNA Isolation Mini kit (Vazyme). The *TRAC* locus target sequences were amplified with Phanta HiFi DNA polymerase (Vazyme) with forward primer-F (GTTGTAAAACGACGGCCAGTGGTACCGCAGTATTATTAAGTAGCCC) and reverse primer-R (CTATGACCATGATTACGCCAAGCTT GTGGCAATGGATAAGGCCGAG). The bands in the size range of 2–3 kb were cut out and purified using a Gel Extraction Kit (Vazyme) and cloned into a pUC57 vector. Individual bacterial colonies were picked for Sanger sequencing. Clones with high-quality sequencing data at both ends were aligned with expected HDR knock-in sequence by BLAST.

Transfection of 293T Cells: For transfection of 293T cells, 25 kDa linear polyethyleneimine (*PEI*) (Polysciences) was used. 1 mg mL^{-1} PEI powder was dissolved in H_2O and adjusted to pH 7.0 with HCl. For 1×10^6 cells in a 6-well plate, 1 µg pX330-RAB, 1 µg template plasmids, and 6 µg PEI (1 mg mL^{-1}, PEI/DNA mass ratio is 3:1) were used.

Cell Viability Assay: Primary human T cells were co-electroporated with template plasmids and RNPs. 72 h after electroporation, T cells were stained with acridine orange (AO) and propidium iodide (PI) mixture (Countstar) at a volume ratio of 1:1, and cell viability was recorded by a Countstar Rigel S3 Fluorescence Cell Analyzer (Countstar).

Antigen Stimulation and Proliferation Assay: CAR-T cells were co-cultured with irradiated NIH/3T3-CD19 cells for weekly stimulation. 2.5×10^5 NIH/3T3-CD19 cells were plated on 24-well tissue culture plates 12 h before addition of 5×10^5 CAR-T cells in X-VIVO 15 supplemented with FBS and cytokines. Total cells were counted and CAR expression was determined weekly by FACS. Subsequently, CAR-T cells were restimulated under the same conditions.

Cell Staining: The following fluorophore-conjugated antibodies were used. From BD Biosciences: PE mouse anti-human CD8; BUV645 mouse anti-human CD4 (Thermo Fisher Scientific); for CAR staining, an Alexa

Fluor 647 AffiniPure F(ab')2 Fragment Goat Anti-Mouse IgG was used (Jackson ImmunoResearch). For TCR staining, a PE Mouse anti-Human CD3 was used (BD Bioscience). For cell counting, CountBright Absolute Counting Beads were added (Thermo Fisher Scientific) according to the manufacturer's instructions.

Cytotoxicity Assay: 9 days after gene targeting, AAV-TRAC-CAR-T cells and p-TRAC-CAR-T cells were stimulated with irradiated NIH/3T3-CD19 cells for a week and then collected for luciferase-based cytotoxicity assay using FFluc-GFP Nalm6 as target cells. The effector (E) and target (T) cells were co-cultured in triplicates at indicated E/T ratios using black 96-well flat plates with 5×10^4 target cells in a total volume of 100 µL per well in RPMI medium. Target cells alone were plated at the same cell density to determine the maximal luciferase expression (relative light units (RLU)); 18 h later, 100 µL luciferase substrate (Goldbio) was directly added to each well. Emitted light was detected in a luminescence plate reader. Lysis was determined as $(1-(\text{RLUsample})/(\text{RLUmax})) \times 100$.

RNA Extraction, Sequencing, and RNAseq Analysis: 7 days after gene targeting, AAV-TRAC-CAR-T cells and p-TRAC-CAR-T cells were stimulated with irradiated NIH/3T3-CD19 for 24 h. RNA was extracted using TRIzol reagent (Thermo Fisher Scientific) followed by chloroform treatment and RNA precipitation by isopropyl alcohol. After RiboGreen RNA quantification and quality control using an Agilent 2100, samples were barcoded and run on a NovaSeq in a 150 base pair (bp)/150 bp paired-end run using the NovaSeq Reagent Kit (Illumina). The raw gene expression counts of each sample were annotated with the "feature Counts" function in the R package "Rsubread" based on the GRCh38 human genome reference. The integrated raw count matrix was then imported into the R package "DESeq2" for downstream analyses, genes with more than 10 raw counts in at least four samples were kept and the filtered raw count matrix was transformed with the "vst" (variance stabilizing transformation) method. These data were then applied for 2D projection with PCA and the scaled expression of selected genes was compared across samples to generate the heat map.

CyTOF Analysis: 9 days after gene targeting, 3×10^6 T cells generated by AAV virus or template plasmids were stimulated with irradiated NIH/3T3-CD19 for 24 h, then harvested together with unstimulated T cells and sent for CyTOF analysis (PLT, Zhejiang, China). In brief, antibodies were either purchased pre-conjugated from Fluidigm (DVS Sciences) or purchased purified and conjugated in-house using MaxPar X8 Polymer Kits (Fluidigm) according to the manufacturer's instructions. Cells for each sample were washed with protein-free phosphate-buffered saline (PBS), stained with 0.25×10^{-6} M Cell-ID Cisplatin-194Pt for 5 min at 4 °C, then incubated with blocking solution for 20 min at 4 °C, then stained for cell surface markers in staining media for 30 min at 4 °C. Cells were fixed and stained with DNA Intercalator-Ir (Fluidigm) overnight. Then intracellular staining was performed for 30 min at room temperature using the Foxp3/Transcription factor staining buffer set (eBioscience), washed, and stored at 4 °C until acquisition. Cells were added with EQ Four Element Calibration Beads (Fluidigm) and analyzed on a Helios instrument. All CyTOF fcs files were uploaded to PLT Biological Information Platform for subsequent analysis. The pre-proceed CyTOF fcs files (fcs 3.0 format) were obtained by standardizing and randomizing the original data. Also, all data were debarcoded using a doublet filtering scheme with mass-tagged barcodes, and then manually gated to retain live, single, valid immune cells by using Flowjo Software. All cell events in each individual sample were pooled in this analysis. Data of all samples were analyzed by machine learning algorithm based on density estimation (Xshift), large-scale data clustering algorithm based on graph theory (PhenoGraph). Finally, the results were displayed by visualization methods such as TiSNE plot, heatmap, density plot, and bar plot.

Mouse Systemic Tumor Model: 6 to 12 weeks old NOD/SCID/IL-2Rγ null mice (Biocytogen, China) were used. All relevant animal-use guidelines and ethical regulations were followed. Mice were inoculated with 0.5×10^6 FFluc-GFP Nalm6 cells by tail vein injection, followed by 1×10^5 CAR-T cells injection 4 days later. Bioluminescence imaging was performed using the IVIS Imaging System (PerkinElmer) with Living Image software (PerkinElmer) for acquisition of imaging datasets. At each indicated time point, three mice from each group were imaged and measured for average tumor burden.

Isolation of Cells from Bone Marrow and Spleen: Mice were euthanized with CO_2 at day 16 and day 36 after CAR-T cell injection. Bone marrow was harvested from freshly isolated femurs and tibiae. After removal of connective tissues and muscles, bones and spleens were crushed in 5 mL PBS-ethylenediaminetetraacetic acid. Single-cell suspensions were made by pipetting and passing supernatant from bone marrow and spleen through a 40 µm filter (BD Falcon). Remaining RBCs were lysed with ACK buffer.

Statistical Analysis: All statistical analyses were performed using the Prism 5 (GraphPad) software. No statistical methods were used to predetermine sample size. Statistical comparisons between two groups were determined by two-tailed paired Student's *t*-test for matched samples. For in vivo experiments, the overall survival was depicted by a Kaplan–Meier curve and the log-rank test was used to compare survival differences between the groups. *p*-Values < 0.05 were considered to be statistically significant. The statistical test used for each figure was described in the corresponding figure legend.

Supporting Information

Supporting Information is available from the Wiley Online Library or from the author.

Acknowledgements

The authors thank the support of Zhejiang Provincial Key Laboratory of Immunity and Inflammatory diseases. The authors thank Zhejiang University School of Medicine core facilities for their support. This research was funded by the National Natural Science Foundation of China grants 31971324 (J.S.) and 31971125 (C.Z.) and by Zhejiang Provincial Natural Science Foundation grant LR20H160003 (J.S.).

Conflict of Interest

A patent application has been submitted based on results presented in this manuscript. R.J., C.Z., and J.S. were listed as the inventors.

Author Contributions

R.J. and P.J. contributed equally to this work. R.J. and P.J. performed the experiments, analyzed, and interpreted the data. X.M., X.W., Y.D., K.S., L.Q., J.C, Y.H., and T.H. performed the experiments. J.L. and W.Y. analyzed the data. J.J., W.C., X.Z., and X.G. interpreted the data. C.Z., M.S., and J.S. designed the study, interpreted the data, and wrote the manuscript.

Data Availability Statement

The data that supports the findings of this study are available in the supplementary material of this article.

Keywords

adoptive cell therapy, CAR, CRISPR/Cas9, genome targeting, nonviral methods, size-reduced plasmid

Received: January 22, 2021
Revised: April 17, 2021
Published online:

[1] C. H. June, M. Sadelain, *N. Engl. J. Med.* **2018**, *379*, 64.
[2] C. Jin, G. Fotaki, M. Ramachandran, B. Nilsson, M. Essand, D. Yu, *EMBO Mol. Med.* **2016**, *8*, 702.
[3] K. K. Haridhasapavalan, M. P. Borgohain, C. Dey, B. Saha, G. Narayan, S. Kumar, R. P. Thummer, *Gene* **2019**, *686*, 146.
[4] P. D. Hsu, E. S. Lander, F. Zhang, *Cell* **2014**, *157*, 1262.
[5] H. Hartweger, A. T. McGuire, M. Horning, J. J. Taylor, P. Dosenovic, D. Yost, A. Gazumyan, M. S. Seaman, L. Stamatatos, M. Jankovic, M. C. Nussenzweig, *J. Exp. Med.* **2019**, *216*, 1301.
[6] Y. Yu, Y. Guo, Q. Tian, Y. Lan, H. Yeh, M. Zhang, I. Tasan, S. Jain, H. Zhao, *Nat. Chem. Biol.* **2020**, *16*, 387.
[7] K. Schumann, S. Lin, E. Boyer, D. R. Simeonov, M. Subramaniam, R. E. Gate, G. E. Haliburton, C. J. Ye, J. A. Bluestone, J. A. Doudna, A. Marson, *Proc. Natl. Acad. Sci. U. S. A.* **2015**, *112*, 10437.
[8] J. Eyquem, J. Mansilla-Soto, T. Giavridis, S. J. van der Stegen, M. Hamieh, K. M. Cunanan, A. Odak, M. Gonen, M. Sadelain, *Nature* **2017**, *543*, 113.
[9] T. L. Roth, C. Puig-Saus, R. Yu, E. Shifrut, J. Carnevale, P. J. Li, J. Hiatt, J. Saco, P. Krystofinski, H. Li, V. Tobin, D. N. Nguyen, M. R. Lee, A. L. Putnam, A. L. Ferris, J. W. Chen, J. N. Schickel, L. Pellerin, D. Carmody, G. Alkorta-Aranburu, D. Del Gaudio, H. Matsumoto, M. Morell, Y. Mao, M. Cho, R. M. Quadros, C. B. Gurumurthy, B. Smith, M. Haugwitz, S. H. Hughes, et al., *Nature* **2018**, *559*, 405.
[10] D. N. Nguyen, T. L. Roth, P. J. Li, P. A. Chen, R. Apathy, M. R. Mamedov, L. T. Vo, V. R. Tobin, D. Goodman, E. Shifrut, J. A. Bluestone, J. M. Puck, F. C. Szoka, A. Marson, *Nat. Biotechnol.* **2020**, *38*, 44.
[11] X. Dai, J. J. Park, Y. Du, H. R. Kim, G. Wang, Y. Errami, S. Chen, *Nat. Methods* **2019**, *16*, 247.
[12] X. Wang, I. Riviere, *Mol. Ther.–Oncolytics* **2016**, *3*, 16015.
[13] E. A. Stadtmauer, J. A. Fraietta, M. M. Davis, A. D. Cohen, K. L. Weber, E. Lancaster, P. A. Mangan, I. Kulikovskaya, M. Gupta, F. Chen, L. Tian, V. E. Gonzalez, J. Xu, I. Y. Jung, J. J. Melenhorst, G. Plesa, J. Shea, T. Matlawski, A. Cervini, A. L. Gaymon, S. Desjardins, A. Lamontagne, J. Salas-Mckee, A. Fesnak, D. L. Siegel, B. L. Levine, J. K. Jadlowsky, R. M. Young, A. Chew, W. T. Hwang, et al., *Science* **2020**, *367*, eaba7365.
[14] J. Zhang, Y. Hu, J. Yang, W. Li, Y. Tian, G. Wei, L. Zhang, K. Zhao, Y. Qi, B. Tan, M. Zhang, Y. Li, Q. Tian, C. Fang, Y. Wu, D. Li, B. Du, M. Liu, H. Huang, MedRxiv.2020.09.22.20199786.
[15] P. K. Mandal, L. M. Ferreira, R. Collins, T. B. Meissner, C. L. Boutwell, M. Friesen, V. Vrbanac, B. S. Garrison, A. Stortchevoi, D. Bryder, K. Musunuru, H. Brand, A. M. Tager, T. M. Allen, M. E. Talkowski, D. J. Rossi, C. A. Cowan, *Cell Stem Cell* **2014**, *15*, 643.
[16] J. J. Albers, T. Ammon, D. Gosmann, S. Audehm, S. Thoene, C. Winter, R. Secci, A. Wolf, A. Stelzl, K. Steiger, J. Ruland, F. Bassermann, C. Kupatt, M. Anton, A. M. Krackhardt, *Life Sci. Alliance* **2019**, *2*, e201900367.
[17] R. O. Bak, D. P. Dever, M. H. Porteus, *Nat. Protoc.* **2018**, *13*, 358.
[18] G. N. Nguyen, J. K. Everett, S. Kafle, A. M. Roche, H. E. Raymond, J. Leiby, C. Wood, C. A. Assenmacher, E. P. Merricks, C. T. Long, H. H. Kazazian, T. C. Nichols, F. D. Bushman, D. E. Sabatino, *Nat. Biotechnol.* **2020**, *39*, 47.
[19] N. A. M. Bakker, R. de Boer, C. Marie, D. Scherman, J. B. A. G. Haanen, J. H. Beijnen, B. Nuijen, J. H. van den Berg, *J. Biotechnol.: X* **2019**, *2*, 100007.
[20] M. Schmeer, T. Buchholz, M. Schleef, *Hum. Gene Ther.* **2017**, *28*, 856.
[21] J. P. Zhang, X. L. Li, G. H. Li, W. Chen, C. Arakaki, G. D. Botimer, D. Baylink, L. Zhang, W. Wen, Y. W. Fu, J. Xu, N. Chun, W. Yuan, T. Cheng, X. B. Zhang, *Genome Biol.* **2017**, *18*, 35.
[22] R. Monjezi, C. Miskey, T. Gogishvili, M. Schleef, M. Schmeer, H. Einsele, Z. Ivics, M. Hudecek, *Leukemia* **2017**, *31*, 186.
[23] X. He, C. Tan, F. Wang, Y. Wang, R. Zhou, D. Cui, W. You, H. Zhao, J. Ren, B. Feng, *Nucleic Acids Res.* **2016**, *44*, e85.
[24] P. Kebriaei, H. Singh, M. H. Huls, M. J. Figliola, R. Bassett, S. Olivares, B. Jena, M. J. Dawson, P. R. Kumaresan, S. Su, S. Maiti, J. Dai, B. Moriarity, M. A. Forget, V. Senyukov, A. Orozco, T. Liu, J. McCarty, R. N. Jackson, J. S. Moyes, G. Rondon, M. Qazilbash, S. Ciurea, A. Alousi, Y. Nieto, K. Rezvani, D. Marin, U. Popat, C. Hosing, E. J. Shpall, et al., *J. Clin. Invest.* **2016**, *126*, 3363.
[25] A. Hendel, R. O. Bak, J. T. Clark, A. B. Kennedy, D. E. Ryan, S. Roy, I. Steinfeld, B. D. Lunstad, R. J. Kaiser, A. B. Wilkens, R. Bacchetta, A. Tsalenko, D. Dellinger, L. Bruhn, M. H. Porteus, *Nat. Biotechnol.* **2015**, *33*, 985.
[26] J. Feucht, J. Sun, J. Eyquem, Y. J. Ho, Z. Zhao, J. Leibold, A. Dobrin, A. Cabriolu, M. Hamieh, M. Sadelain, *Nat. Med.* **2019**, *25*, 82.
[27] H. Dai, Z. Wu, H. Jia, C. Tong, Y. Guo, D. Ti, X. Han, Y. Liu, W. Zhang, C. Wang, Y. Zhang, M. Chen, Q. Yang, Y. Wang, W. Han, *J. Hematol. Oncol.* **2020**, *13*, 30.
[28] N. N. Shah, B. D. Johnson, D. Schneider, F. Zhu, A. Szabo, C. A. Keever-Taylor, W. Krueger, A. A. Worden, M. J. Kadan, S. Yim, A. Cunningham, M. Hamadani, T. S. Fenske, B. Dropulic, R. Orentas, P. Hari, *Nat. Med.* **2020**, *26*, 1569.